

# STAR-RIS Enhanced UAV-Enabled MEC Networks with Bi-Directional Task Offloading

Han Xiao, *Student Member, IEEE*, Xiaoyan Hu\*, *Member, IEEE*,  
Pengcheng Mu, *Member, IEEE*, Weile Zhang, *Member, IEEE*, Wenjie Wang, *Member, IEEE*,  
Kai-Kit Wong, *Fellow, IEEE*, Kun Yang, *Fellow, IEEE*

**Abstract**—A simultaneously transmitting and reflecting reconfigurable intelligent surface (STAR-RIS) enhanced unnamed aerial vehicle (UAV)-enabled multi-user mobile edge computing (MEC) scheme is proposed in this paper. Different from the existing MEC works, the proposed scheme allows bi-directional offloading where users can simultaneously offload their computing tasks to the MEC servers situated at the ground base station (BS) and aerial UAV with the assistance of the STAR-RIS. Specifically, we formulate an optimization problem aiming at maximizing the energy efficiency of the system while ensuring the quality of service (QoS) constraint by jointly optimizing the resource allocation, user scheduling, passive beamforming of the STAR-RIS, and the UAV trajectory. An iterative algorithm designed with the Dinkelbach's algorithm and the successive convex approximation (SCA) is proposed to effectively handle the formulated non-convex optimization problem. Simulation results indicate that the proposed STAR-RIS enhanced UAV-enabled MEC scheme possesses significant advantages in enhancing the system energy efficiency over other baseline schemes including the conventional RIS-aided scheme.

**Index Terms**—STAR-RIS, unnamed aerial vehicle (UAV), mobile edge computing (MEC), energy efficiency.

## I. INTRODUCTION

Nowadays, the number of wireless devices is experiencing an exponential explosive growth, and the applications of the Internet of Things (IoT) are becoming increasingly diverse. As for the implementation of those computation-intensive and latency-critical applications, e.g., autonomous driving, augmented and virtual reality, etc., it presents significant challenges for the widely used center-cloud computing framework to effectively handle large amounts of data in swift actions. [1]–[3]. To address this challenge, the technology of mobile edge computing (MEC) has emerged as a promising solution for effectively tackling the significantly augmented computational necessity, which is able to bring the capabilities of cloud computing to the network edge. The technology of MEC enables data processing in close proximity, and thus it performs well in reducing network congestion, and improving service quality and user experience [4]–[6]. While the MEC

technology provides an effective means to enhance the network computing capabilities, the traditional placement strategy for MEC servers near the ground base stations (BSs) or access points (APs) may result in a limited service coverage.

To overcome this limitation, the unmanned aerial vehicles (UAVs) are leveraged to assist the task completion of the MEC networks due to the inherent advantages of UAVs, such as exceptional mobility and flexibility [7]–[14]. Specifically, in [7], the UAV is equipped with a MEC server acting as an aerial MEC platform to facilitate the computation of the offloaded tasks for users with low-quality transmission links from the BSs or APs. In [8], the UAV is leveraged as a relay to support the transfer of users' computational tasks to the MEC servers located at BS. The authors in [9] introduce a novel MEC scheme that involves both aerial and ground cooperation. The proposed scheme enables users to efficiently offload their task data to multiple base stations (BSs) and unmanned aerial vehicles (UAVs) in a collaborative manner. Furthermore, a two-way offloading UAV-aided MEC scheme is proposed in [10]–[12] to enhance the computing capacity of the MEC network, where the UAV not only carries the MEC processor but also serves as a relay to facilitate the offloading of tasks from users to ground MEC servers. Although UAV is able to effectively improve the computing capacity of MEC networks, the existing UAV-aided MEC schemes are designed by adapting to uncontrollable random wireless channels, which seriously limits the task offloading efficiency.

A promising solution to tackle this issue is the reconfigurable intelligent surface (RIS) technique [15]. Due to the fact that RIS can dynamically adjust the phases and amplitudes of incident signals, allowing the creation of controllable end-to-end virtual channels, RIS has been incorporated into various kinds of communication systems including MEC networks [16]–[19]. It is important to highlight that UAVs flying at high altitudes enables the establishment of a reliable line-of-sight (LoS) connection between the UAV and users with a high possibility. Additionally, RIS technology has the capability to reconfigure the wireless propagation environment, and thus combining UAV and RIS will be a win-win strategy for MEC networks. In particular, a RIS-assisted UAV-enabled MEC scheme considering the aim of maximizing energy efficiency is proposed in [17]. In [18], the UAV-mounted RIS scheme is proposed to assist MEC network, where users can only offload their tasks to ground MEC servers with the help of the reflected ability of the RIS. To further improve the computational capacity of the MEC network, a two-way offloading scheme

H. Xiao, X. Hu, P. Mu, W. Zhang and W. Wang are with the School of Information and Communications Engineering, Xi'an Jiaotong University, Xi'an 710049, China. (email: hanxiaonuli@stu.xjtu.edu.cn, xiaoyanhu@xjtu.edu.cn, {pcmu, wlzhang, wjwang}@mail.xjtu.edu.cn).

K.-K. Wong is with the Department of Electronic and Electrical Engineering, University College London, London WC1E 7JE, U.K. (email: kai-kit.wong@ucl.ac.uk)

K. Yang is with the School of Computer Science and Electronic Engineering, University of Essex, Colchester CO4 3SQ, U.K. (e-mail: kun-yang@essex.ac.uk).

assisted by the UAV and the RIS is proposed in [19], [20]. In this scheme, a multi-antenna UAV is responsible for processing a portion of the computation tasks and acts as a relay to transmit the remaining tasks to the BS in the next time slot.

Actually, the existing UAV-enabled MEC schemes usually leverage a two-step task offloading strategy to achieve two-way task offloading to the BS and UAV, which have certain limitations: (i) The UAV serves as multiple roles where it acts as an MEC platform for processing partial offloaded tasks, and a relay to send the remaining tasks to the BS, which imposes a challenge on UAV hardware design. (ii) These two-step MEC schemes are not energy and time efficient since the UAV needs to receive all the offloaded tasks, and then transmit the unprocessed tasks to the BS. Hence, it is challenging for the traditional RIS-assisted UAV-enabled MEC schemes to offload users' tasks to both the BS and the UAV simultaneously in a more efficient manner [19], [20]. Recently, an advanced RIS technology, named as simultaneously transmitting and reflecting reconfigurable intelligent surface (STAR-RIS), has drawn great attention from both academia and industry [21], [22]. STAR-RIS can split the incident signal into two parts, where one part is reflected to the same side of the incident signal and the other part is transited to the opposite side, allowing a 360° coverage, compared with the conventional RIS. Due to the inherent advantages, STAR-RIS possesses an enormous application potentials in various wireless communication systems, e.g., [23]–[26]. Hence, to enhance the current MEC schemes, we try to incorporate the STAR-RIS into UAV-assisted MEC networks, allowing the simultaneously bi-directional offloading strategy for the cooperation between the UAV and the BS. In this paper, our main contributions are summarized as follows:

- **STAR-RIS enhanced UAV-enabled MEC Architecture with Bi-directional Offloading:** In this paper, a novel MEC scheme aided by STAR-RIS and UAV is proposed for the first time. In contrast to the existing UAV-enabled MEC schemes, the proposed scheme allows users to simultaneously offload their computing tasks to the MEC servers located at the BS and UAV in a bi-directional manner through the reflection and transmission capabilities of the STAR-RIS. Note that the UAV in the proposed MEC scheme is solely responsible for carrying the MEC server and the STAR-RIS to assist the computation and offloading of users' tasks.
- **Optimization Problem Formulation Maximizing Energy Efficiency under Practical Constraints:** We formulate optimization problem with the aim of maximizing the energy efficiency of the system and ensuring users' quality of service (QoS) constraints by jointly designing the resource allocation, users scheduling, passive beamforming and UAV trajectory. Actually, managing this optimization problem can be quite difficult because of the presence of a fractional objective function and the significant couplings among optimization variables.
- **Iterative Algorithm with Guaranteed Convergence and Substantial Performance Gain:** To effectively address this non-convex optimization problem, the alternative

strategy is leveraged to divide the optimization problem into three subproblems. Then, an iterative algorithm based on the Dinkelbach's algorithm [27, Chapter 3.2.1] and the successive convex approximation (SCA) technique is proposed to effectively solve these three subproblems. The convergence of the proposed algorithm can be guaranteed, which has also been confirmed through simulation results. Moreover, the performance improvement and potential applications of the STAR-RIS enhanced UAV-enabled MEC scheme are demonstrated by comparing the simulation results with three other baseline schemes, including the conventional RIS-aided scheme.

The remainder of this paper is organized as follows. In Section II, the system model of the STAR-RIS enhanced UAV-enabled MEC network is presented, along with the channel models, task offloading and computation models, as well as the energy consumption model of the system. The formulated optimization problem and the designed iterative algorithm are shown in Section III, including the convergence and complexity analysis of the proposed algorithm. The numerical simulation is conducted in Section IV to verify the effectiveness of the designed algorithm and the proposed MEC scheme. Finally, the conclusion is made in Section V.

*Notation:* Operator  $\circ$  denotes the Hadamard product.  $(\cdot)^T$ ,  $(\cdot)^H$  and  $(\cdot)^*$  represent transpose, conjugate transpose and conjugate, respectively.  $\text{Diag}(\mathbf{a})$  denotes a diagonal matrix with diagonal elements in vector  $\mathbf{a}$  while  $\text{diag}(\mathbf{A})$  denotes a vector whose elements are composed of the diagonal elements of matrix  $\mathbf{A}$ .  $|\cdot|$ ,  $\|\cdot\|$  indicate the complex modulus and the spectral norm, respectively. Operator  $\text{norm}(\mathbf{a})$  will normalize the amplitude of all entities in vector  $\mathbf{a}$  as 1.

## II. SYSTEM MODEL

Fig. 1 shows the UAV-enabled MEC network assisted by STAR-RIS, which mainly consists of a ground base station (BS),  $K$  ground users each with a single antenna, a aerial UAV equipped with a signal antenna and mounted a STAR-RIS with  $M$  elements, two MEC servers respectively located at the BS and UAV. In this letter, the energy splitting protocol is executed for STAR-RIS, signifying that all elements integrated into the STAR-RIS possess the capability to simultaneously reflect (R) and transmit (T) the incident signals [21]. This characteristic implies that users can offload their computing tasks in a bi-directional manner, simultaneously to the MEC server located at the BS using the R mode of the STAR-RIS, as well as to the MEC server mounted on the UAV using the T mode.

In this paper, we divide the mission period  $T$  into  $N$  equal time slots, i.e.,  $\delta_t = T/N$ , which is sufficiently small. We assume that the UAV is equipped with a transceiver that has a single antenna and the time division multiple access (TDMA) protocol is implemented to handle users' offloaded tasks, indicating that only one user will be chosen to offload their computing tasks to the BS and the UAV within a time slot. Hence, we use the variable  $\zeta_k[n] \in \{0, 1\}$  for  $k \in \mathcal{K} \triangleq \{1, \dots, k, \dots, K\}$ ,  $n \in \mathcal{N} \triangleq \{1, \dots, n, \dots, N\}$  to represent the user association decision for task offloading in a time slot. In particular, if  $\zeta_k[n] = 1$ , it means that the  $k$ -th

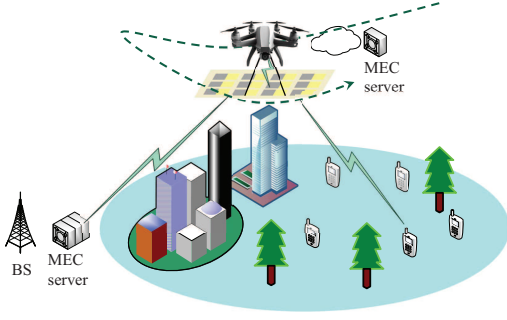


Fig. 1. The UAV-enabled MEC network with bi-directional offloading strategy supported by the STAR-RIS.

user is chosen to offload its task to the BS and UAV in the  $n$ -th time slot with the assistance of the STAR-RIS. Additionally, variable  $\zeta_k[n]$  needs to satisfy the following constraint:

$$\sum_{k=1}^K \zeta_k[n] = 1, \quad \zeta_k[n] \in \{0, 1\}, \quad \forall k \in \mathcal{K}, n \in \mathcal{N}. \quad (1)$$

In order to clearly describe the considered scenario, we assume that all nodes are situated in a 3D Cartesian coordinate system. The positions of the BS and the  $k$ -th user are respectively denoted as  $\mathbf{q}_{\text{BS}} = [x_{\text{BS}}, y_{\text{BS}}, z_{\text{BS}}]^T$  and  $\mathbf{q}_k = [x_k, y_k, 0]^T$ , where  $x_{\text{BS}}$  and  $x_k$  respectively denote the abscissa value of the BS and the  $k$ -th user,  $y_{\text{BS}}$  and  $y_k$  respectively represent the vertical coordinates of the BS and the  $k$ -th user,  $z_{\text{BS}}$  is the height of the BS. It is assumed that the UAV flies at a fixed altitude  $H$  and its position remains constant within a given time slot considering the small value of  $\delta_t$ . Consequently, the location of the UAV in the  $n$ -th time slot can be represented as  $\mathbf{q}_{\text{ua}}[n] = [x_{\text{ua}}[n], y_{\text{ua}}[n], H]^T$ ,  $n \in \mathcal{N}$ , which should adhere to the subsequent flight constraints:

$$\mathbf{v}_{\text{ua}}[n] = \frac{\mathbf{q}_{\text{ua}}[n+1] - \mathbf{q}_{\text{ua}}[n]}{\delta_t}, \quad \|\mathbf{v}_{\text{ua}}[n]\| \leq v_{\text{max}}, \quad (2)$$

$$\mathbf{a}_{\text{ua}}[n] = \frac{\mathbf{v}_{\text{ua}}[n+1] - \mathbf{v}_{\text{ua}}[n]}{\delta_t}, \quad \|\mathbf{a}_{\text{ua}}[n]\| \leq a_{\text{max}}, \quad (3)$$

$$\mathbf{q}_{\text{ua}}[0] = \mathbf{q}_{\text{I}}, \quad \mathbf{q}_{\text{ua}}[N+1] = \mathbf{q}_{\text{F}}, \quad (4)$$

where  $\|\mathbf{v}_{\text{ua}}[n]\|$  and  $\|\mathbf{a}_{\text{ua}}[n]\|$  respectively represent the flight speed and the acceleration of the UAV in the  $n$ -th time slot, with the maximum values of  $v_{\text{max}}$  and  $a_{\text{max}}$ . In terms of  $\mathbf{q}_{\text{I}}$  and  $\mathbf{q}_{\text{F}}$ , these locations can serve as the ground station where the UAV can access a reliable power supply and receive necessary maintenance.

#### A. Channel Model

Due to the fact that the UAV flights at a high altitude, we assume that the line-of-sight (LoS) channels between the ground users/BS and aerial UAV/STAR-RIS can always be guaranteed. It is assumed that the STAR-RIS adopts the uniform planar array (UPA) with  $M_x$  elements along  $x$ -axis direction and  $M_y$  elements along  $y$ -axis direction, i.e.,  $M = M_x M_y$ . Hence, the channel between the  $k$ -th user ( $\varsigma = \text{rk}$ )/BS ( $\varsigma = \text{rb}$ ) and the

STAR-RIS in the  $n$ -th time slot for  $k \in \mathcal{K}$ ,  $n \in \mathcal{N}$  can be expressed as [28]

$$\mathbf{h}_{\varsigma}[n] = \sqrt{\frac{\rho}{d_{\varsigma}^{\alpha_{\varsigma}}[n]}} \widehat{\mathbf{h}}_{\varsigma}[n], \quad \varsigma \in \{\text{rk}, \text{rb}\}, \quad (5)$$

where

$$\widehat{\mathbf{h}}_{\varsigma}[n] = [1, \dots, e^{-j\frac{2\pi d}{\lambda}(m_x-1)\xi_{\varsigma}[n]}, \dots, e^{-j\frac{2\pi d}{\lambda}(M_x-1)\xi_{\varsigma}[n]}]^T \otimes [1, \dots, e^{-j\frac{2\pi d}{\lambda}(m_y-1)\chi_{\varsigma}[n]}, \dots, e^{-j\frac{2\pi d}{\lambda}(M_y-1)\chi_{\varsigma}[n]}]^T, \quad (6)$$

with  $\rho = (\frac{\lambda}{4\pi})^2$  and  $\lambda$  being the wavelength of the carrier frequency,  $\alpha_{\varsigma}$  indicating the pass loss exponent,  $d_{\varsigma}[n]$  denoting the distance between  $k$ -th user/BS and the STAR-RIS.  $d$  denotes the adjacent element separation of the STAR-RIS. In addition, the  $\xi_{\varsigma}[n]$  and  $\chi_{\varsigma}[n]$  corresponding to the  $k$ -th user and the BS are respectively calculated as

$$\xi_{\text{rk}}[n] = \cos(\phi_{\text{rk}}[n]) \sin(\theta_{\text{rk}}[n]) = \frac{x_{\text{ua}}[n] - x_k}{\|\mathbf{q}_{\text{ua}}[n] - \mathbf{q}_k\|}, \quad (7)$$

$$\xi_{\text{rb}}[n] = \cos(\phi_{\text{rb}}[n]) \sin(\theta_{\text{rb}}[n]) = \frac{x_{\text{BS}} - x_{\text{ua}}[n]}{\|\mathbf{q}_{\text{BS}} - \mathbf{q}_{\text{ua}}[n]\|}, \quad (8)$$

$$\chi_{\text{rk}}[n] = \sin(\phi_{\text{rk}}[n]) \sin(\theta_{\text{rk}}[n]) = \frac{y_{\text{ua}}[n] - y_k}{\|\mathbf{q}_{\text{ua}}[n] - \mathbf{q}_k\|}, \quad (9)$$

$$\chi_{\text{rb}}[n] = \sin(\phi_{\text{rb}}[n]) \sin(\theta_{\text{rb}}[n]) = \frac{y_{\text{BS}} - y_{\text{ua}}[n]}{\|\mathbf{q}_{\text{BS}} - \mathbf{q}_{\text{ua}}[n]\|}. \quad (10)$$

It is important to note that the connection between the UAV and STAR-RIS should be described as the near-field channel, denoted as  $\mathbf{h}_{\text{ru}}$ , considering the fact that the distance between the UAV and STAR-RIS is extremely small. Thus,  $\mathbf{h}_{\text{ru}}$  can be expressed as [29]

$$\mathbf{h}_{\text{ru}} = \boldsymbol{\alpha} \circ \mathbf{a}_{\text{ru}}, \quad (11)$$

where

$$\begin{aligned} \bullet \quad \boldsymbol{\alpha} &= \left[ \frac{\lambda}{4\pi r_1}, \dots, \frac{\lambda}{4\pi r_m}, \dots, \frac{\lambda}{4\pi r_M} \right]^T, \\ \bullet \quad \mathbf{a}_{\text{ru}} &= \left[ e^{-j\frac{2\pi r_1}{\lambda}}, \dots, e^{-j\frac{2\pi r_m}{\lambda}}, \dots, e^{-j\frac{2\pi r_M}{\lambda}} \right]^T, \end{aligned}$$

with  $r_m$  being the distance between the antenna at UAV and the  $m$ -th element equipped at STAR-RIS. It is worth noting that the channel  $\mathbf{h}_{\text{ru}}$  remains constant due to the fixed relative position between the UAV and the STAR-RIS.

#### B. Task Offloading and Computation Model

The offloading rates achieved by the  $k$ -th user in the  $n$ -th time slot to the BS and UAV are respectively given by

$$R_k^{\text{ua}}[n] = \zeta_k[n] B \log_2 \left( 1 + \frac{p \left| \mathbf{h}_{\text{ru}}^H \boldsymbol{\Theta}_t^H[n] \mathbf{h}_{\text{rk}}[n] \right|^2}{\sigma_{\text{ua}}^2} \right), \quad (12)$$

$$R_k^{\text{BS}}[n] = \zeta_k[n] B \log_2 \left( 1 + \frac{p \left| \mathbf{h}_{\text{ru}}^H[n] \boldsymbol{\Theta}_r^H[n] \mathbf{h}_{\text{rk}}[n] \right|^2}{\sigma_{\text{BS}}^2} \right), \quad (13)$$

where  $p$  denotes the unified transmitted power of users,  $B$  is the bandwidth of the system,  $\sigma_{\text{ua}}^2$  and  $\sigma_{\text{BS}}^2$  respectively denote the noise power at the BS and the UAV. In addition,  $\boldsymbol{\Theta}_{\kappa}[n] = \text{Diag} \{ \beta_{\kappa}^1[n] e^{j\phi_{\kappa}^1[n]}, \dots, \beta_{\kappa}^m[n] e^{j\phi_{\kappa}^m[n]}, \dots, \beta_{\kappa}^M[n] e^{j\phi_{\kappa}^M[n]} \}$

is the matrix of the STAR-RIS's coefficients with  $\kappa \in \{r, t\}$  representing the reflected or transmitted coefficients of the STAR-RIS, where the amplitudes  $\beta_\kappa^m[n]$  and phases  $\phi_\kappa^m[n]$  of the STAR-RIS should satisfy  $(\beta_r^m[n])^2 + (\beta_t^m[n])^2 = 1$ ,  $\phi_r^m[n], \phi_t^m[n] \in [0, 2\pi], \forall m \in \mathcal{M} \triangleq \{1, \dots, m, \dots, M\}$ .

We assume that the ground users are with limited resources for local computing and thus users' tasks have to be offloaded to the BS and UAV for computing. Let  $l_k^{\text{BS}}[n]$  and  $l_k^{\text{ua}}[n]$  denote the number of the offloaded bits that need to be computed at the BS and UAV for user  $k$  in the  $n$ -th time slot, respectively. Due to the fact that the BS and UAV can only deal with the tasks they have received, the following constraints should be satisfied

$$\delta_t \zeta_k[n] R_k^{\text{ua}}[n] \geq l_k^{\text{ua}}[n], \quad \forall k \in \mathcal{K}, n \in \mathcal{N}, \quad (14)$$

$$\delta_t \zeta_k[n] R_k^{\text{BS}}[n] \geq l_k^{\text{BS}}[n], \quad \forall k \in \mathcal{K}, n \in \mathcal{N}. \quad (15)$$

In order to ensure that every user's minimum computational need is met, we implement the following QoS constraint

$$\sum_{n=1}^N (l_k^{\text{BS}}[n] + l_k^{\text{ua}}[n]) \geq L_k, \quad \forall k \in \mathcal{K}, \quad (16)$$

where  $L_k$  is the minimum computing tasks of the  $k$ -th user.

Let  $f_k^{\text{BS}}[n]$  and  $f_k^{\text{ua}}[n]$  respectively denote the computation frequency allocated by the BS and UAV for the  $k$ -th user at the  $n$ -th time slot, we have

$$\sum_{k=1}^K f_k^{\text{BS}}[n] \leq F_{\text{BS}}, \quad \sum_{k=1}^K f_k^{\text{ua}}[n] \leq F_{\text{ua}}, \quad \forall n \in \mathcal{N}, \quad (17)$$

where  $F_{\text{BS}}$  and  $F_{\text{ua}}$  are the maximum CPU frequency at the BS and the UAV, respectively. In addition, considering the processing causality, it is assumed that the BS and the UAV solely receive the offloaded tasks without carrying out any computations within the first time slot, and the users cease the act of offloading their tasks at the last time slot, i.e.,  $f_k^{\text{BS}}[1] = f_k^{\text{ua}}[1] = l_k^{\text{BS}}[N] = l_k^{\text{ua}}[N] = 0$  for  $k \in \mathcal{K}$ . In order to guarantee that all users' offloaded task-input data can be completely computed within the give mission time  $T$ , we have the following information-causality constraints:

$$\sum_{i=2}^n \frac{f_k^{\text{ua}}[i] \delta_t}{\varrho_{\text{ua}}} \geq \sum_{i=1}^{n-1} l_k^{\text{ua}}[i], \quad \forall k \in \mathcal{K}, n \in \mathcal{N}_1, \quad (18)$$

$$\sum_{i=2}^n \frac{f_k^{\text{BS}}[i] \delta_t}{\varrho_{\text{BS}}} \geq \sum_{i=1}^{n-1} l_k^{\text{BS}}[i], \quad k \in \mathcal{K}, \forall n \in \mathcal{N}_1, \quad (19)$$

where  $\varrho_{\text{BS}}$  and  $\varrho_{\text{ua}}$  represent the number of CPU cycles needed for processing 1-bit of task-input data at the BS and UAV, respectively, and  $\mathcal{N}_1 \triangleq \{2, 3, \dots, N\}$  is a subset of  $\mathcal{N}$ . Therefore, the total amount of the completed task-input data for all users within the whole period can be calculated as

$$L_{\text{tol}} = \sum_{n=1}^N \sum_{k=1}^K l_k^{\text{BS}}[n] + l_k^{\text{ua}}[n], \quad (20)$$

which is an important indicator to measure the computing capability of the MEC system.

### C. Energy Consumption Model

The energy consumption in the system primarily occurs in three ways: task offloading by users, task computation by the BS and UAV, and the UAV's flying process. Specifically, the energy consumed by users to offload tasks during the total mission period is given by

$$E_{\text{ut}} = p \delta_t (N - 1), \quad (21)$$

considering the fact that only the first  $N - 1$  time slots are utilized by users for task offloading.

According to [10], the energy consumption of the MEC servers situated at the BS and the UAV for computing the received tasks within the whole mission period  $T$  can be respectively expressed as

$$E_{\text{BS}}^{\text{com}} = \sum_{n=1}^N \sum_{k=1}^K \iota_{\text{BS}} \delta_t (f_k^{\text{BS}}[n])^3, \quad (22)$$

$$E_{\text{ua}}^{\text{com}} = \sum_{n=1}^N \sum_{k=1}^K \iota_{\text{ua}} \delta_t (f_k^{\text{ua}}[n])^3, \quad (23)$$

where  $\iota_{\text{BS}}$  and  $\iota_{\text{ua}}$  are the effective capacitance coefficients of the MEC servers at the BS and the UAV, respectively.

In this paper, we select the rotary-wing UAV to enhance the STAR-RIS-assisted UAV-enabled MEC network. Consequently, the flying energy consumed by the UAV during the mission period can be expressed as [30]

$$E_{\text{ua}}^{\text{fly}} = \sum_{n=1}^N \delta_t \left( P_0 \left( 1 + \frac{3v^2[n]}{U_{\text{tip}}^2} \right) + \frac{1}{2} \mu \psi q A v^3[n] \right. \\ \left. + \hat{P}_0 \sqrt{\left( 1 + \frac{v^4[n]}{4v_0^4} \right)^{\frac{1}{2}} - \frac{v^2[n]}{2v_0^2}} \right), \quad (24)$$

where  $P_0$  and  $\hat{P}_0$  denote the blade profile power and induced power in the hovering status, respectively.  $U_{\text{tip}}$ ,  $\mu$ ,  $\psi$ ,  $q$ ,  $A$  and  $v_0$  are parameters related to the UAV's aerodynamics, and more details are presented in Table I of [30]. It is worth noting that  $v[n] = \|\mathbf{v}_{\text{ua}}[n]\|$  represents the flight velocity of the UAV at the  $n$ -th time slot.

In this paper, the energy consumption of the BS in processing an computing the received tasks is not taken into account for optimization and analysis, due to the fact that the BS is usually adequately supplied with grid power. Hence, the system's energy consumption is represented by the total energy used by the UAV and all users, given as

$$E_{\text{tol}} = E_{\text{ut}} + E_{\text{ua}}^{\text{com}} + E_{\text{ua}}^{\text{fly}}, \quad (25)$$

which is also an important performance indicator to measure the MEC system.

## III. PROBLEM FORMULATION AND ALGORITHM DESIGN

### A. Optimization Problem Formulation

In this section, the optimization problem will be formulated based on the analysis in Section II. In particular, we try to maximize the energy efficiency of the MEC system, defined as  $\frac{L_{\text{tol}}}{E_{\text{tol}}}$ , which takes both the indicators of computing capability  $L_{\text{tol}}$  and the energy consumption  $E_{\text{tol}}$  into consideration,

while ensuring the QoS constraints of users with minimum computational requirements, by jointly optimizing

- the resource allocation variables in  $\mathbf{L} \triangleq \{l_k^{\text{ua}}[n], l_k^{\text{BS}}[n], f_k^{\text{ua}}[n], f_k^{\text{BS}}[n], k \in \mathcal{K}, n \in \mathcal{N}\}$ ;
- the user scheduling variables for task offloading in  $\zeta \triangleq \{\zeta_k[n], k \in \mathcal{K}, n \in \mathcal{N}\}$ ;
- the passive beamforming variables of STAR-RIS in  $\Upsilon \triangleq \{\Theta_r[n], \Theta_t[n], n \in \mathcal{N}\}$ ;
- the UAV trajectory variables in  $\mathbf{Q} \triangleq \{\mathbf{q}_{\text{ua}}[n], n \in \mathcal{N}\}$ .

Hence, the corresponding optimization problem can be formulated as

$$\begin{aligned} \max_{\mathbf{L}, \zeta, \Upsilon, \mathbf{Q}} \quad & \frac{L_{\text{tol}}}{E_{\text{tol}}}, \\ \text{s.t.} \quad & (14) - (19), \end{aligned} \quad (26a)$$

$$\|\mathbf{v}_{\text{ua}}[n]\| \leq v_{\text{max}}, \|\mathbf{a}_{\text{ua}}[n]\| \leq a_{\text{max}}, \forall n \in \mathcal{N}, \quad (26b)$$

$$\mathbf{q}_{\text{ua}}[0] = \mathbf{q}_{\text{I}}, \mathbf{q}_{\text{ua}}[N] = \mathbf{q}_{\text{F}}, \quad (26c)$$

$$\sum_{k=1}^K \zeta_k[n] = 1, \zeta_k[n] \in \{0, 1\}, n \in \mathcal{N}, k \in \mathcal{K}, \quad (26d)$$

$$f_k^{\text{ua}}[1] = f_k^{\text{BS}}[1] = l_k^{\text{ua}}[N] = l_k^{\text{BS}}[N] = 0, \forall k \in \mathcal{K}, \quad (26e)$$

$$(\beta_r^m[n])^2 + (\beta_t^m[n])^2 = 1, \forall m \in \mathcal{M}, n \in \mathcal{N}, \quad (26f)$$

$$\beta_r^m[n], \beta_t^m[n] \in (0, 1), \forall m \in \mathcal{M}, n \in \mathcal{N}, \quad (26g)$$

$$\phi_r^m[n], \phi_t^m[n] \in [0, 2\pi), \forall m \in \mathcal{M}, n \in \mathcal{N}. \quad (26h)$$

Actually, the problem (26) is a non-convex problem due to the non-convexity of the objective function, and constraints (14), (15) and (26f), which is difficult to solve directly. To overcome this challenge, the alternative strategy is employed to divide the original optimization problem into three subproblems. The algorithm is designed by alternatively optimizing three variable subsets, which are respectively denoted as  $\Xi_1 = \{\mathbf{L}, \zeta\}$ ,  $\Xi_2 = \{\mathbf{L}, \Upsilon\}$  and  $\Xi_3 = \{\mathbf{L}, \mathbf{Q}\}$ . More details of the algorithm design is given in the next subsection.

## B. Algorithm Design

1) *Designing  $\Xi_1$  with the given  $\mathbf{Q}$  and  $\Upsilon$* : First, we jointly optimize the resource allocation variable  $\mathbf{L}$  and user scheduling variable  $\zeta$  with the given passive beamforming and UAV trajectory. In this case, the original problem (26) can be simplified as

$$\begin{aligned} \max_{\Xi_1} \quad & \frac{L_{\text{tol}}(\Xi_1)}{E_{\text{tol}}(\Xi_1)} \\ \text{s.t.} \quad & (26a), (26d), (26e). \end{aligned} \quad (27a)$$

Note that the optimization problem (27) is still a non-convex problem because of the fractional objective function and the binary variable  $\zeta$ . To tackle this problem, we first leverage the Dinkelbach's algorithm [27, Chapter 3.2.1] to transform the fractional objective function. Specifically, the objective function in the  $(l+1)$ -th iteration of the Dinkelbach's algorithm can be expressed as

$$\hat{\gamma}^{(l+1)} = L_{\text{tol}}(\Xi_1) - \psi^{(l)} E_{\text{tol}}(\Xi_1), \quad (28)$$

where  $\psi^{(l)}$  can be updated with  $\psi^{(l)} = \frac{L_{\text{tol}}(\Xi_1^{(l)})}{E_{\text{tol}}(\Xi_1^{(l)})}$ .

In terms of the non-convex binary constraint (26d), we equivalently transform it into the following constraints:

$$\begin{aligned} \sum_{k=1}^K \zeta_k[n] &= 1, 0 \leq \zeta_k[n] \leq 1, \forall n \in \mathcal{N}, k \in \mathcal{K}, \quad (29) \\ \eta_k[n] &= \zeta_k[n] - \zeta_k^2[n] = 0, \forall n \in \mathcal{N}, k \in \mathcal{K}. \quad (30) \end{aligned}$$

Note that for any  $\zeta_k[n] \in [0, 1]$ ,  $\eta_k[n] \geq 0$  always holds and the equality in (29) is satisfied if and only if  $\zeta_k[n] = 0$  or  $\zeta_k[n] = 1$ . Considering the non-negative characteristic of  $\{\eta_k[n]\}_{k \in \mathcal{K}, n \in \mathcal{N}}$ , we try to add the sum of them into the objective function as a penalty term that is subtracted from the objective function. To guarantee the fulfilment of the binary constraint (26d), an additional inner loop iteration is incorporated into the  $(l+1)$ -th iteration of the Dinkelbach's algorithm to iteratively enforce the penalty term approaching to 0. Note that the inclusion of the penalty term in the objective function results in a non-concave objective function due to the convex nature of  $-\eta_k[n]$  with respect to (w.r.t.)  $\zeta_k[n]$ . To handle this problem, we utilize the liner upper bound, i.e., the first-order Taylor expansion of  $\eta_k[n]$ , to replace itself. The liner upper bound of  $\eta_k[n]$  in the  $(t+1)$ -th inner loop iteration can be expressed as

$$\begin{aligned} \bullet \quad \eta_k[n] &\leq \hat{\eta}_k[n](\zeta_k[n], \zeta_k^{(t)}[n]) = \zeta_k[n] - ((\zeta_k^{(t)}[n])^2 + 2\zeta_k^{(t)}[n](\zeta_k[n] - \zeta_k^{(t)}[n])). \end{aligned}$$

Thus, in the  $(t+1)$ -th inner loop iteration of the  $(l+1)$ -th iteration of the Dinkelbach's algorithm, the optimization problem (27) can be re-expressed

$$\begin{aligned} \max_{\Xi_1} \quad & \hat{\gamma}^{(l+1)} - \hat{\rho} \sum_{n=1}^N \sum_{k=1}^K \hat{\eta}_k[n](\zeta_k[n], \zeta_k^{(t)}[n]) \\ \text{s.t.} \quad & (26a), (26e), (29), \end{aligned} \quad (31a)$$

where  $\hat{\rho} > 0$  denotes the introduced penalty coefficient. The problem (31) is a convex optimization problem and can be directly solved by the existing tool such as CVX.

To solve problem (27), we propose a two-tier iterative algorithm which is summarized as Algorithm 1. The primary objective of the outer loop is to modify the fractional objective function using the Dinkelbach's algorithm. On the other hand, the inner loop aims to ensure that the binary constraint is met by progressively increasing the penalty coefficient with  $\hat{\rho} = \omega \hat{\rho}$ , where  $\omega > 1$  is the scaling factor.

2) *Designing  $\Xi_2$  with given  $\zeta$  and  $\mathbf{Q}$* : After achieving the user scheduling  $\zeta$ , we focus on designing the passive beamforming variables with the given UAV's trajectory. In particular, the corresponding optimization problem for passive beamforming can be expressed as

$$\begin{aligned} \max_{\Xi_2} \quad & \frac{L_{\text{tol}}(\Xi_2)}{E_{\text{tol}}(\Xi_2)} \\ \text{s.t.} \quad & (26a), (26e) - (26h). \end{aligned} \quad (32a)$$

Note that, problem (32) is a non-convex optimization problem because of the non-convexity of the fractional objective function and constraints (14), (15) and (26f). However, we can derive the close form expression of the optimal reflected and transmitted phases according to the following Theorem 1.

*Theorem 1. The obtained optimal reflection and transmission phases at the  $n$ -th time slot can be given by*

$$\phi_r[n] = \arg(\text{norm}(\mathbf{h}_{rb}^*[n] \circ \mathbf{h}_{rk}[n])), \quad (33)$$

$$\phi_t[n] = \arg(\text{norm}(\mathbf{h}_{ru}^*[n] \circ \mathbf{h}_{rk}[n])), \quad (34)$$

where the selection of the index  $k$  is determined by the condition of  $\zeta_k[n] = 1$ .

*Proof.* To maximize the achievable offloaded rates  $R_k^{\text{ua}}[n]$  and  $R_k^{\text{BS}}[n]$  when  $\zeta_k[n] = 1$  in the  $n$ -th time slot, the optimal phases of the STAR-RIS's passive beamforming can be determined by utilizing the maximum ratio transmission (MRT) technique.  $\square$

---

**Algorithm 1:** The Proposed Iterative Algorithm for Solving the Sub-problem (27)

---

- 1: Initialize the feasible point  $(\mathbf{L}^{(0,0)}, \zeta^{(0,0)})$ ; Define the tolerance accuracy thresholds as  $\varepsilon$  and  $\hat{\varepsilon}$ ; Set the outer iteration index  $l = 0$ .
  - 2: **While**  $v_1 > \varepsilon_1$  or  $l = 0$  **do**
  - 3: Set the inner iteration index  $t = 0$ ; Initialize  $\hat{\rho}^{(0)}$ .
  - 4: **While**  $v_2 > \varepsilon_2$  or  $t = 0$  **do**
  - 5: Solve the optimization problem (31) with the given  $(\mathbf{L}_b^{(l,t)}, \zeta^{(l,t)})$  and update  $(\mathbf{L}_b^{(l,t+1)}, \zeta^{(l,t+1)})$  with the obtained solutions.
  - 6: Calculate  $v_2 = \max_{k \in \mathcal{K}, n \in \mathcal{N}} \eta_k[n]$  based on the acquired solutions; Update the penalty coefficients  $\hat{\rho} = \omega \hat{\rho}$ ; Let  $t = t + 1$ .
  - 7: **end while**
  - 8: Update  $(\mathbf{L}_b^{(l+1,0)}, \zeta^{(l+1,0)})$  with  $(\mathbf{L}_b^{(l,t)}, \zeta^{(l,t)})$ .
  - 9: Calculate  $v_1 = L_{\text{tol}}^{(l+1)} - \psi^{(l)} E_{\text{tol}}^{(l+1)}$  based on the acquired solution;
  - 10: Calculate the  $\psi^{(l+1)} = \frac{L_{\text{tol}}(\mathbf{L}_b^{(l+1,0)}, \zeta^{(l+1,0)})}{E_{\text{tol}}(\mathbf{L}_b^{(l+1,0)}, \zeta^{(l+1,0)})}$ ; Let  $l = l + 1$ .
  - 12: **end while**
- 

Next, we will focus on designing the reflection and transmission amplitudes of STAR-RIS's passive beamforming, i.e.,  $\{\beta_\kappa^m[n]\}_{m \in \mathcal{M}, n \in \mathcal{N}}$ . In terms of the fractional objective function, similarly, we resort to the Dinkelbach's algorithm to transform it. For the non-convex constraints (14) and (15), we first rewrite  $\vartheta_\kappa[n] = \Phi_\kappa[n] \beta_\kappa[n]$ ,  $\kappa \in \{r, t\}$ , where we have  $\vartheta_\kappa[n] = \text{diag}(\Theta_\kappa[n])$ ,  $\beta_\kappa[n] = \{\beta_\kappa^1[n], \dots, \beta_\kappa^m[n], \dots, \beta_\kappa^M[n]\}^T$ , and  $\Phi_\kappa[n] = \text{Diag}(e^{j\phi_\kappa[n]})$ . Therefore,  $R_k^{\text{BS}}[n]$  and  $R_k^{\text{ua}}[n]$  can be further re-expressed as

$$R_k^{\text{BS}}[n] = \zeta_k[n] B \log_2 \left( 1 + \beta_r^T[n] \mathbf{F}_k[n] \beta_r[n] \right), \quad (35)$$

$$R_k^{\text{ua}}[n] = \zeta_k[n] B \log_2 \left( 1 + \beta_t^T[n] \mathbf{E}_k[n] \beta_t[n] \right), \quad (36)$$

where

- $\mathbf{F}_k[n] = \frac{\Phi_r^H[n]}{\sigma_{\text{BS}}^2} (\mathbf{h}_{\text{BR}}^*[n] \circ \mathbf{h}_{rk}[n]) (\mathbf{h}_{\text{BR}}^*[n] \circ \mathbf{h}_{rk}[n])^H \Phi_r[n]$ ,
- $\mathbf{E}_k[n] = \frac{\Phi_t^H[n]}{\sigma_{\text{ua}}^2} (\mathbf{h}_{\text{ru}}^*[n] \circ \mathbf{h}_{rk}[n]) (\mathbf{h}_{\text{ru}}^*[n] \circ \mathbf{h}_{rk}[n])^H \Phi_t[n]$ .

Then, we introduce auxiliary variables  $\gamma_k^{\text{BS}}[n]$  and  $\gamma_k^{\text{ua}}[n]$  which satisfy  $\gamma_k^{\text{BS}}[n] \leq \beta_r^T[n] \mathbf{F}_k[n] \beta_r[n]$  and  $\gamma_k^{\text{ua}}[n] \leq \beta_t^T[n] \mathbf{E}_k[n] \beta_t[n]$ . Thus, the problem designing reflection and transmission amplitudes in the  $(\hat{t} + 1)$ -th iteration of the Dinkelbach's algorithm can be equivalently transformed as

$$\max_{\beta_r, \beta_t, \gamma} L_{\text{tol}}(\beta_r, \beta_t, \gamma) - \hat{\psi}^{(\hat{t})} E_{\text{tol}}(\beta_r, \beta_t, \gamma)$$

$$\text{s.t. (16) - (19), (26e),} \quad (37a)$$

$$\delta_t[n] \zeta_k[n] \log_2(1 + \gamma_k^{\text{ua}}[n]) \geq l_k^{\text{ua}}[n], \quad \forall k \in \mathcal{K}, n \in \mathcal{N}, \quad (37b)$$

$$\delta_t[n] \zeta_k[n] \log_2(1 + \gamma_k^{\text{BS}}[n]) \geq l_k^{\text{BS}}[n], \quad \forall k \in \mathcal{K}, n \in \mathcal{N}, \quad (37c)$$

$$\gamma_k^{\text{ua}}[n] \leq \beta_t^T[n] \mathbf{E}_k[n] \beta_t[n], \quad \forall k \in \mathcal{K}, n \in \mathcal{N}, \quad (37d)$$

$$\gamma_k^{\text{BS}}[n] \leq \beta_r^T[n] \mathbf{F}_k[n] \beta_r[n], \quad \forall k \in \mathcal{K}, n \in \mathcal{N}, \quad (37e)$$

$$(\beta_r^m[n])^2 + (\beta_t^m[n])^2 \leq 1, \quad \forall m \in \mathcal{M}, n \in \mathcal{N}. \quad (37f)$$

where  $\gamma \triangleq \{\gamma_k^{\text{ua}}[n], \gamma_k^{\text{BS}}[n], k \in \mathcal{K}, n \in \mathcal{N}\}$ . Actually, problem (37) is still a non-convex optimization problem due to the non-convex constraints (37d) and (37e). In order to address this issue, we employ a linear lower bound, specifically the first-order Taylor expansion, to approximate the right-hand side of constraints (37d) and (37e) and replace them accordingly. Note that the equality sign in constraint (26f) is replaced with an inequality sign to form constraint (37f). In fact, this change does not impact the fulfilment of the equality constraint, because the constraint (37f) is satisfied with strict equality in the optimal solution of problem (37). Consequently, we can obtain a convex optimization problem.

3) *Designing  $\Xi_3$  with given  $\zeta$  and  $\Upsilon$ :* Next, we will design the trajectory of the UAV with the obtained  $\zeta$  and  $\Upsilon$ . Specifically, the corresponding optimization problem for UAV trajectory can be expressed as

$$\max_{\Xi_3} \frac{L_{\text{tol}}(\Xi_3)}{E_{\text{tol}}(\Xi_3)}, \quad \text{s.t. (26a) - (26c), (26e).} \quad (38a)$$

In fact, problem (38) is non-convex because of the objective function and constraints (14) and (15). Similarly, we utilize the Dinkelbach's algorithm to transform the fractional objective function. In order to handle this non-convex constraints, we first introduce the auxiliary variables  $\lambda_k[n]$  and  $\tilde{\lambda}[n]$  with

$$\lambda_k[n] \geq d_{rk}^{\alpha_{rk}}[n] = \|\mathbf{q}_{\text{ua}}[n] - \mathbf{q}_k\|^{\alpha_{rk}}, \quad (39)$$

$$\tilde{\lambda}[n] \geq d_{\text{rb}}^{\alpha_{\text{rb}}}[n] = \|\mathbf{q}_{\text{BS}} - \mathbf{q}_{\text{ua}}[n]\|^{\alpha_{\text{rb}}}. \quad (40)$$

Hence, we have

$$R_k^{\text{ua}}[n] \geq \tilde{R}_k^{\text{ua}}[n] = \log_2 \left( 1 + \frac{\rho p \left| \mathbf{h}_{\text{ru}}^H \Theta_t^H[n] \hat{\mathbf{h}}_{\text{uk}}[n] \right|^2}{\lambda_k[n] \sigma_{\text{ua}}^2} \right), \quad (41)$$

$$R_k^{\text{BS}}[n] \geq \tilde{R}_k^{\text{BS}}[n] = \log_2 \left( 1 + \frac{\rho^2 p_k[n] \left| \hat{\mathbf{h}}_{\text{BR}}^H[n] \Theta_r^H[n] \hat{\mathbf{h}}_{\text{uk}}[n] \right|^2}{\lambda_k[n] \tilde{\lambda}[n] \sigma_{\text{ua}}^2} \right). \quad (42)$$

Actually,  $\tilde{R}_k^{\text{ua}}[n]$  is a convex function w.r.t.  $\lambda_k[n]$  and  $\tilde{R}_k^{\text{BS}}[n]$  is the jointly convex function w.r.t.  $\lambda_k[n]$  and  $\tilde{\lambda}[n]$ , and thus we can apply the first-order Taylor expansion of  $\tilde{R}_k^{\text{ua}}[n]$  and

$\widehat{R}_k^{\text{BS}}[n]$  at the given point  $(\lambda_k^{(s)}[n], \tilde{\lambda}^{(s)}[n])$  in  $(s+1)$ -th iteration of the Dinkelbach's algorithm to convert constraints (14) and (15) as the following convex constraints

$$\zeta_k[n] \delta_t \widehat{R}_k^{\text{ua}}[n] \geq l_k^{\text{ua}}[n], \quad \forall k \in \mathcal{K}, n \in \mathcal{N}, \quad (43)$$

$$\zeta_k[n] \delta_t \widehat{R}_k^{\text{BS}}[n] \geq l_k^{\text{BS}}[n], \quad \forall k \in \mathcal{K}, n \in \mathcal{N}, \quad (44)$$

where

- $\widehat{R}_k^{\text{ua}}[n] = \log_2 \left( 1 + \frac{\rho p |\mathbf{h}_{\text{ru}}^H \Theta_t^H [n] \widehat{\mathbf{h}}_{\text{rk}}[n]|^2}{\lambda_k^{(s)}[n] \sigma_{\text{ua}}^2} \right) + (\lambda_k[n] - \lambda_k^{(s)}[n]) f(\lambda_k^{(s)}[n]).$
- $\widehat{R}_k^{\text{BS}}[n] = (\lambda_k[n] - \lambda_k^{(s)}[n]) \tilde{f}_1(\lambda_k^{(s)}[n], \tilde{\lambda}^{(s)}[n]) + (\tilde{\lambda}[n] - \tilde{\lambda}^{(s)}[n]) \tilde{f}_2(\lambda_k^{(s)}[n], \tilde{\lambda}^{(s)}[n]) + \log_2 \left( 1 + \frac{\rho^2 p |\widehat{\mathbf{h}}_{\text{BR}}^H [n] \Theta_r^H [n] \widehat{\mathbf{h}}_{\text{rk}}[n]|^2}{\lambda_k^{(s)}[n] \tilde{\lambda}^{(s)}[n] \sigma_{\text{ua}}^2} \right).$
- $f(\lambda_k^{(s)}[n]) = \frac{-\rho p |\mathbf{h}_{\text{ru}}^H \Theta_t^H [n] \widehat{\mathbf{h}}_{\text{rk}}[n]|^2}{\ln 2 (\rho p |\mathbf{h}_{\text{ru}}^H \Theta_t^H [n] \widehat{\mathbf{h}}_{\text{rk}}[n]|^2 + \lambda_k^{(s)}[n] \sigma_{\text{ua}}^2) \lambda_k^{(s)}[n]}.$
- $\tilde{f}_1(\lambda_k^{(s)}[n], \tilde{\lambda}^{(s)}[n]) = \frac{-\rho^2 p |\widehat{\mathbf{h}}_{\text{BR}}^H [n] \Theta_r^H [n] \widehat{\mathbf{h}}_{\text{rk}}[n]|^2}{\ln 2 \lambda_k^{(s)}[n] (\rho^2 p |\widehat{\mathbf{h}}_{\text{BR}}^H [n] \Theta_r^H [n] \widehat{\mathbf{h}}_{\text{rk}}[n]|^2 + \lambda_k^{(s)}[n] \tilde{\lambda}^{(s)}[n] \sigma_{\text{ua}}^2)}.$
- $\tilde{f}_2(\lambda_k^{(s)}[n], \tilde{\lambda}^{(s)}[n]) = \frac{-\rho^2 p |\widehat{\mathbf{h}}_{\text{BR}}^H [n] \Theta_r^H [n] \widehat{\mathbf{h}}_{\text{rk}}[n]|^2}{\ln 2 \tilde{\lambda}^{(s)}[n] (\rho^2 p |\widehat{\mathbf{h}}_{\text{BR}}^H [n] \Theta_r^H [n] \widehat{\mathbf{h}}_{\text{rk}}[n]|^2 + \lambda_k^{(s)}[n] \tilde{\lambda}^{(s)}[n] \sigma_{\text{ua}}^2)}.$

Note that,  $E_{\text{tol}}$  is a non-convex function w.r.t. variable  $\mathbf{Q}$  due to the non-convexity of  $E_{\text{ua}}^{\text{fly}}$ . To tackle this problem, we further introduce a non-negative auxiliary variable  $\widehat{\mu}[n]$  with  $\widehat{\mu}^2[n] \geq (1 + \frac{v^4[n]}{4v_0^4})^{\frac{1}{2}} - \frac{v^2[n]}{2v_0^2}$  to obtain the upper bound of  $E_{\text{ua}}^{\text{fly}}$ , which is expressed as

$$\begin{aligned} \widehat{E}_{\text{ua}}^{\text{fly}} &= \sum_{n=1}^N \delta_t \left( P_0 \left( 1 + \frac{3v^2[n]}{U_{\text{tip}}^2} \right) + \frac{1}{2} \mu \psi q A v^3[n] \right. \\ &\quad \left. + \widehat{P}_0 \widehat{\mu}[n] \right). \end{aligned} \quad (45)$$

Actually, the introduced constraint  $\widehat{\mu}^2[n] \geq (1 + \frac{v^4[n]}{4v_0^4})^{\frac{1}{2}} - \frac{v^2[n]}{2v_0^2}$  is a non-convex constraint. To handle this non-convex constraint, we first equivalently transform it as  $\widehat{\mu}^2[n] + \frac{v^2[n]}{v_0^2} \geq \frac{1}{\widehat{\mu}^2[n]}$ . Note that  $\widehat{\mu}^2[n] + \frac{v^2[n]}{v_0^2}$  is a jointly convex function w.r.t.  $\widehat{\mu}[n]$  and  $v[n]$ , so the first-order Taylor expansion can be utilized to transform this constraint, and thus we have

$$\begin{aligned} g(\widehat{\mu}, v[n]) &= (\widehat{\mu}^{(s)}[n])^2 + 2\mu^{(s)}[n] (\widehat{\mu}[n] - \widehat{\mu}^{(s)}[n]) \\ &\quad + \frac{2}{v_0^2 \delta_t^2} (\mathbf{q}_{\text{ua}}^{(s)}[n+1] - \mathbf{q}_{\text{ua}}^{(s)}[n])^T (\mathbf{q}_{\text{ua}}[n+1] - \mathbf{q}_{\text{ua}}[n]) \\ &\quad - \frac{\left\| \mathbf{q}_{\text{ua}}^{(s)}[n+1] - \mathbf{q}_{\text{ua}}^{(s)}[n] \right\|^2}{v_0^2 \delta_t^2} \geq \frac{1}{\widehat{\mu}^2[n]}. \end{aligned} \quad (46)$$

As a result, the optimization problem (38) in the  $(s+1)$ -th iteration of the Dinkelbach's algorithm can be transformed as

$$\max_{\Xi} \quad \mathbf{L}(\Xi) - \tau^{(s+1)} \widehat{E}_{\text{tol}}(\Xi),$$

$$\text{s.t. (16) - (19), (26b), (26c), (26e), (43), (44), (46),} \quad (47a)$$

$$\lambda_k[n] \geq \|\mathbf{q}_{\text{ua}}[n] - \mathbf{q}_k\|^{\alpha_{\text{rk}}}, \quad (47b)$$

$$\tilde{\lambda}[n] \geq \|\mathbf{q}_{\text{BS}} - \mathbf{q}_{\text{ua}}[n]\|^{\alpha_{\text{rb}}}, \quad (47c)$$

where  $\Xi = \{\Xi_3, \lambda_k[n], \tilde{\lambda}[n], \mu[n]\}$ ,  $\widehat{E}_{\text{tol}} = \widehat{E}_{\text{ua}}^{\text{fly}} + E_{\text{ut}} + E_{\text{ua}}^{\text{com}}$ . Consequently, we can leverage the convex optimization solver, e.g., CVX, to address this problem.

### C. Proposed Optimization Algorithm & Analysis on Complexity and Convergence

The presented iterative algorithm for solving the original optimization problem (26) is summarized as Algorithm 2, which is a block coordinate descent (BCD) algorithm designed to tackle the three subproblems explained in Section III. The value  $v$  represents the difference of the obtained objective function value between adjacent iterations. Once  $v$  falls below a predefined threshold  $\varepsilon$ , the proposed algorithm will converge.

---

#### Algorithm 2: Proposed Iterative Algorithm to Handle the Optimization Problem (26)

---

- 1: Initialize feasible point  $(\mathbf{L}^{(0)}, \zeta^{(0)}, \Upsilon^{(0)}, \mathbf{Q}^{(0)})$ ; Define the tolerance accuracy threshold  $\varepsilon$ ; Set the outer iteration index  $\widehat{l} = 0$ .
  - 2: **While**  $v > \varepsilon$  or  $\widehat{l} = 0$  **do**
  - 3: Solve the sub-problem (27) by utilizing Algorithm 1 with the given  $\Upsilon^{(\widehat{l})}$  and  $\mathbf{Q}^{(\widehat{l})}$ , and update  $\mathbf{L}^{(\widehat{l}+1)}$  and  $\zeta^{(\widehat{l}+1)}$  with the obtained solution.
  - 4: Solve the sub-problem (37) based on the Dinkelbach's algorithm with the given  $\zeta^{(\widehat{l}+1)}$  and  $\mathbf{Q}^{(\widehat{l})}$ , and update  $\mathbf{L}^{(\widehat{l}+1)}$  and  $\Upsilon^{(\widehat{l}+1)}$  with the obtained solution.
  - 5: Solve the sub-problem (47) based on the Dinkelbach's algorithm with the given  $\zeta^{(\widehat{l}+1)}$  and  $\Upsilon^{(\widehat{l}+1)}$ , and update  $\mathbf{L}^{(\widehat{l}+1)}$  and  $\mathbf{Q}^{(\widehat{l}+1)}$  with the obtained solution.
  - 6: Calculate the objective value  $\overline{R}^{(\widehat{l}+1)} = \frac{L_{\text{tol}}^{(\widehat{l}+1)}}{E_{\text{tol}}^{(\widehat{l}+1)}}$  and update  $v = \left| \overline{R}^{(\widehat{l}+1)} - \overline{R}^{(\widehat{l})} \right|$  based the obtained solutions; Let  $\widehat{l} = \widehat{l} + 1$ .
  - 7: **end while**
- 

Then, the computational complexity of the proposed iterative algorithm is analysed. Specifically, the computational complexity mainly comes from solving the divided three subproblems, i.e., (27), (32) and (38). Regarding the first subproblem, we propose a two-tier algorithm that incorporates both Dinkelbach's algorithm and the penalty method to effectively address it. It is presumed that the interior point method will be employed to compute the transformed standard convex optimization problem. Consequently, the computational complexity for resolving the first subproblem can be expressed as  $\mathcal{O}_1 = \mathcal{O}(L_1 L_2 (5NK)^{3.5})$ , where  $L_1$  and  $L_2$  denote the number of iterations in the outer and inner loops, respectively. In terms of the subproblem designing the passive beamforming, the computational complexity is dominated by handling the optimization problem (37), which is given by  $\mathcal{O}_2 = \mathcal{O}(L_3 (4NK + 2M)^{3.5})$ , where  $L_3$  is the number of iteration. For the subproblem 3, the SCA technique is adopted to transform the UAV trajectory problem into a convex optimization problem. Supposing  $L_4$  is the

number of iteration, the the computational complexity can be determined as  $\mathcal{O}_3 = \mathcal{O}(L_4(4NK + 2N)^{3.5})$ . Therefore, the total computing complexity of the proposed algorithm can be expressed as  $\mathcal{O}_{\text{tot}} = L(\mathcal{O}_1 + \mathcal{O}_2 + \mathcal{O}_2)$ , where  $L$  denotes the total iteration number of the proposed algorithm. Based on the overall computational complexity analysis, it is evident that the computing complexity is intricately connected to both the quantity of sub-time slots ( $N$ ) and the number of elements installed at STAR-RIS ( $M$ ).

Actually, the convergence of the proposed algorithm can be guaranteed by utilizing the BCD algorithm to address the optimization problem (26). Because this approach ensures that each iteration results in a solution that is at least as good as the previous one and thus the objective function is monotonically non-decreasing versus the iteration. Additionally, we will also verify the convergence of the proposed algorithm through the simulation results presented in Section IV.

#### IV. SIMULATION RESULTS

To highlight the effectiveness of the proposed STAR-RIS-aided UAV-enabled MEC scheme, we present the numerical simulation results in this section and compare the their with three benchmark schemes, including: **1) RIS-aided scheme [23]:** In this baseline scheme, two adjacent conventional RISs with  $\frac{M}{2}$  elements are adopted to replace the STAR-RIS, where one is the reflecting-only RIS and the other one is the transmission-only RIS; **2) Without trajectory optimization scheme:** This scheme focuses on optimizing  $\mathbf{L}$ ,  $\zeta$  and  $\Upsilon$  with direct UAV trajectory flying from the initial point to the final point at a consistent speed. **3) Heuristic scheme:** UAV will traverse each user node based on the pre-defined trajectory at a consistent speed. Similarly, variables  $\mathbf{L}$ ,  $\zeta$  and  $\Upsilon$  will be optimized in this scheme. In addition, the simulation parameters are listed in Table I.

TABLE I  
PARAMETERS SETTING

Parameters	Symbol and Value
Altitude of UAV	$H = 30$ m
Bandwidth	$B = 1$ MHz
Carrier frequency	$\lambda_c = 2.4$ GHz
Effective capacitance coefficient of MEC servers	$\iota_{\text{ua}} = \iota_{\text{BS}} = 10^{-27}$
Initial/final point of UAV trajectory	$\mathbf{q}_I = [-40, 0, 30]^T$ m, $\mathbf{q}_F = [40, 0, 30]^T$ m
Maximum flight velocity and acceleration of UAV	$v_{\text{max}} = 30$ m/s, $a_{\text{max}} = 20$ m/s <sup>2</sup>
Maximum CPU frequency	$F_{\text{BS}} = 20$ GHz, $F_{\text{ua}} = 12$ GHz
Noise power	$\sigma_{\text{ua}}^2 = \sigma_{\text{BS}}^2 = -100$ dBm
Pass loss exponent	$\alpha_{\text{rk}} = 2.3$ , $\alpha_{\text{rb}} = 2.3$
Scaling factor	$\omega = 10$
The number of CPU cycles needed for processing 1-bit of data	$\varrho_{\text{ua}} = \varrho_{\text{BS}} = 10^3$ cycles/bit
Time slot	$\delta_t = 0.2$ s
Transmitting power at users	$p = 20$ dBm,
Tolerance accuracy thresholds	$\varepsilon = \varepsilon_1 = \varepsilon_2 = 10^{-3}$

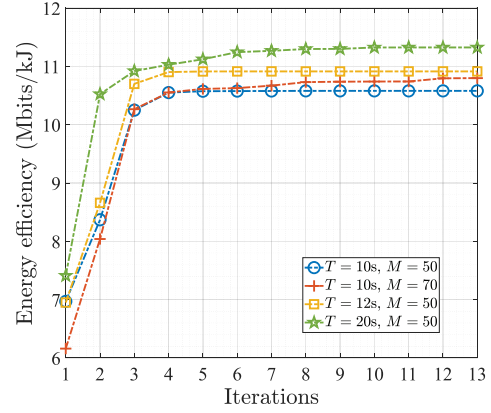


Fig. 2. Energy efficiency versus iterations index with  $L_k = 20$  Mbits, with different mission period  $T$  and the number of elements at STAR-RIS  $M$ .

In order to assess the convergence of the proposed algorithm, we examine the performance of energy efficiency w.r.t. the number of iteration, which is shown in Fig. 2, taking into account of various mission periods  $T$  and the STAR-RIS's number of elements  $M$ . The outcomes of this investigation are illustrated in Figure 2. Specifically, it is observed that the energy efficiency monotonically increasing with the iteration index and ultimately converges to a specific value. In terms of the four cases under consideration, it is noteworthy that the objective function consistently attains a stable value within a relatively short span of 5-6 iterations.

In Fig. 3 and Fig. 4, we give the UAV trajectories considering different parameter settings, where  $M$  is fixed as 36. Specifically, UAV trajectories under different mission period  $T$  and time slot number  $N$  are shown in Fig. 3, where all the users with computation requirements  $L_k = 20$  Mbits. We can find that the UAV consistently flies towards User 3, who is the furthest user away from the BS, in order to improve the channel quality between User 3 and the BS under different  $T$ . This is done to ensure that User 3's minimum task requirement is met. Additionally, it demonstrates that the UAV tends to approach the BS as  $T$  increases, which aims to offload larger tasks to the BS, ultimately enhancing the energy efficiency. In Fig. 4, the UAV trajectories is plotted with different  $\{L_k\}_{k \in \mathcal{K}}$ . It is observed that when all users share the same minimum task requirement, the UAV prioritizes traversing users located at longer distances from the BS, such as User 1, User 2, and User 3. However, if certain users, like User 3 and User 5, require a higher number of offloading task bits, the UAV will approach these users to improve their channel quality and fulfil their task requirements.

Next, we investigate the influence of the number of elements equipped at STAR-RIS, i.e.,  $M$ , on the energy efficiency with  $N = 50$  and  $L_k = 20$  Mbits,  $\forall k \in \mathcal{K}$ . Specifically, it can be observed that the energy efficiency of all the schemes increases as  $M$  grows, as the additional elements can offer more flexibility to reconfigure the wireless environment. However, the rates of increase gradually decrease as  $M$  continues to grow. The proposed scheme offers a greater performance gain in improving the energy efficiency, especially when the number of elements is limited, compared to the conventional



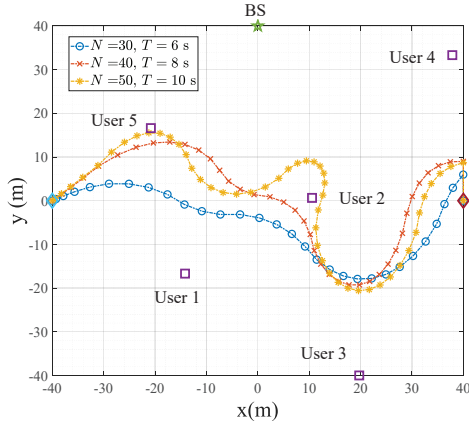


Fig. 3. UAV trajectory with  $M = 36$  and  $L_k = 20$  Mbits, as well as the different mission period  $T$  and  $N$ .

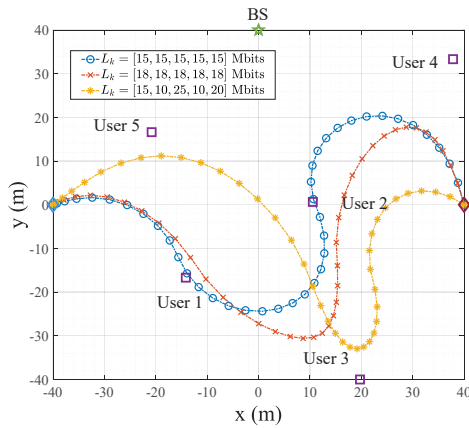


Fig. 4. UAV trajectory with different  $L_k$ , with  $T = 10$  s,  $N = 50$  and  $M = 36$ .

RIS-assisted scheme. Additionally, an interesting observation is obtained between the RIS-aided scheme and the heuristic scheme. Specifically, the heuristic scheme achieves higher energy efficiency than the RIS-aided scheme when the  $M$  is small. As  $M$  increases, the RIS-aided scheme becomes more energy efficient than the heuristic scheme. This indicates that the trajectory of the UAV, with the help of the RIS, has the potential to overcome performance limitations imposed by other system settings. These observations are also evident when comparing with the heuristic scheme.

Fig. 6 explores the impact of the mission duration  $T$  on energy efficiency when  $M$  is fixed at 50 and  $L_k$  is set to 20 Mbits  $\forall k \in \mathcal{K}$ . The results show that the proposed scheme provides the highest performance gain for MEC network, while the scheme without the trajectory optimization exhibits the lowest energy efficiency. Regarding the proposed scheme, the energy efficiency consistently increases as  $T$  grows from 8s to 18s. This can be attributed to the fact that the UAV having more time to optimize its trajectory, thereby improving the channel condition between users/BS and UAV as  $T$  increases. However, beyond 18s, the energy efficiency starts to decline. This is due to the channel quality between users/BS and UAV reaching a saturation point, which may not increase the completed task bits but increase the energy consumption of

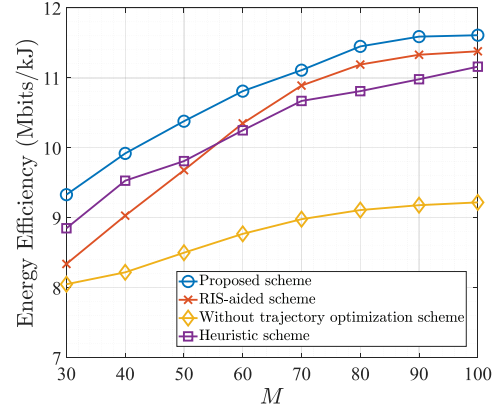


Fig. 5. Energy efficiency versus the number of elements at STAR-RIS with  $N = 50$  and  $L_k = 20$  Mbits,  $\forall k \in \mathcal{K}$ .

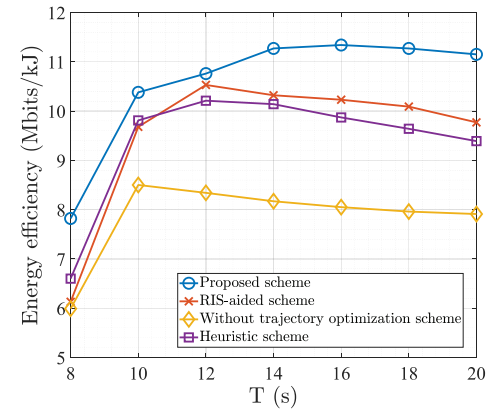


Fig. 6. Energy efficiency versus the mission period  $T$  with  $M = 50$  and  $L_k = 20$  Mbits,  $\forall k \in \mathcal{K}$ .

UAV as  $T$  becomes larger. Besides, the conventional RIS-assisted scheme has the similar trend in energy efficiency as the proposed scheme. However, the energy efficiency reaches the limitation at  $T = 12$ s in this scheme, which indicates that STAR-RIS demonstrates a significant potential in achieving a balance between system energy consumption and the volume of the offloaded data when compared to the conventional RIS. In contrast to the suggested scheme, both the heuristic scheme and the scheme with direct UAV trajectory suffer from the earlier performance limitation as  $T$  increases. This highlights the significance of the UAV's trajectory optimization in augmenting the energy efficiency of the comprehensive UAV-enabled MEC system.

## V. CONCLUSION

In this paper, we propose a MEC scheme assisted by STAR-RIS and UAV, which allows the bi-directional task offloading so that users can offload their tasks to the MEC servers situated at the BS and UAV simultaneously. A non-convex optimization problem is established which seeks to maximize the energy efficiency while guaranteeing the QoS constraints for users. In order to effectively address this non-convex optimization problem, we propose an iterative algorithm that draws inspiration from the Dinkelbach's algorithm

and the SCA technique. The proposed iterative algorithm can effectively solve the established problem with guaranteed convergence. The efficacy of the proposed MEC scheme is substantiated through the simulation outcomes in comparison with the several existing baseline schemes, encompassing the traditional RIS-assisted scheme.

## REFERENCES

- [1] Y. Mao, C. You, J. Zhang, K. Huang, and K. B. Letaief, "A survey on mobile edge computing: The communication perspective," *IEEE Commun. Surveys & Tuts.*, vol. 19, no. 4, pp. 2322–2358, 2017.
- [2] X. Hu, K.-K. Wong, C. Masouros, and S. Jin, "IRS-Aided Mobile Edge Computing: From Optimization to Learning," *Intelligent Surfaces Empowered 6G Wireless Network*, 2023.
- [3] A. Al-Fuqaha, M. Guizani, M. Mohammadi, M. Aledhari, and M. Ayyash, "Internet of things: A survey on enabling technologies, protocols, and applications," *IEEE Commun. Surveys & Tuts.*, vol. 17, no. 4, pp. 2347–2376, 2015.
- [4] X. Hu, K.-K. Wong, and K. Yang, "Wireless powered cooperation-assisted mobile edge computing," *IEEE Trans. Wireless Commun.*, vol. 17, no. 4, pp. 2375–2388, 2018.
- [5] C. You, K. Huang, H. Chae, and B.-H. Kim, "Energy-efficient resource allocation for mobile-edge computation offloading," *IEEE Trans. Wireless Commun.*, vol. 16, no. 3, pp. 1397–1411, 2016.
- [6] S. Bi and Y. J. Zhang, "Computation rate maximization for wireless powered mobile-edge computing with binary computation offloading," *IEEE Trans. Wireless Commun.*, vol. 17, no. 6, pp. 4177–4190, 2018.
- [7] S. Jeong, O. Simeone, and J. Kang, "Mobile edge computing via a UAV-mounted cloudlet: Optimization of bit allocation and path planning," *IEEE Trans. Veh. Technol.*, vol. 67, no. 3, pp. 2049–2063, 2017.
- [8] X. Gu, G. Zhang, M. Wang, W. Duan, M. Wen, and P.-H. Ho, "UAV-aided energy-efficient edge computing networks: Security offloading optimization," *IEEE Internet Things J.*, vol. 9, no. 6, pp. 4245–4258, 2021.
- [9] Y. Xu, T. Zhang, Y. Liu, D. Yang, L. Xiao, and M. Tao, "UAV-assisted MEC networks with aerial and ground cooperation," *IEEE Trans. Wireless Commun.*, vol. 20, no. 12, pp. 7712–7727, 2021.
- [10] X. Hu, K.-K. Wong, K. Yang, and Z. Zheng, "UAV-assisted relaying and edge computing: Scheduling and trajectory optimization," *IEEE Trans. Wireless Commun.*, vol. 18, no. 10, pp. 4738–4752, 2019.
- [11] X. Hu, K.-K. Wong, and Y. Zhang, "Wireless-powered edge computing with cooperative UAV: Task, time scheduling and trajectory design," *IEEE Wireless Commun.*, vol. 19, no. 12, pp. 8083–8098, 2020.
- [12] T. Zhang, Y. Xu, J. Loo, D. Yang, and L. Xiao, "Joint computation and communication design for UAV-assisted mobile edge computing in IoT," *IEEE Trans. Ind. Informat.*, vol. 16, no. 8, pp. 5505–5516, 2019.
- [13] J. Zhang, L. Zhou, F. Zhou, B.-C. Seet, H. Zhang, Z. Cai, and J. Wei, "Computation-efficient offloading and trajectory scheduling for multi-UAV assisted mobile edge computing," *IEEE Trans. Vehicular Technol.*, vol. 69, no. 2, pp. 2114–2125, 2019.
- [14] Z. Yang, M. Chen, X. Liu, Y. Liu, Y. Chen, S. Cui, and H. V. Poor, "AI-driven UAV-NOMA-MEC in next generation wireless networks," *IEEE Wireless Commun.*, vol. 28, no. 5, pp. 66–73, 2021.
- [15] C. Huang, A. Zappone, G. C. Alexandropoulos, M. Debbah, and C. Yuen, "Reconfigurable intelligent surfaces for energy efficiency in wireless communication," *IEEE Trans. Wireless Commun.*, vol. 18, no. 8, pp. 4157–4170, 2019.
- [16] X. Hu, C. Masouros, and K.-K. Wong, "Reconfigurable intelligent surface aided mobile edge computing: From optimization-based to location-only learning-based solutions," *IEEE Trans. Commun.*, vol. 69, no. 6, pp. 3709–3725, 2021.
- [17] X. Qin, Z. Song, T. Hou, W. Yu, J. Wang, and X. Sun, "Joint Optimization of Resource Allocation, Phase Shift and UAV Trajectory for Energy-Efficient RIS-Assisted UAV-Enabled MEC Systems," *IEEE Trans. Green Commun. Netw.*, 2023.
- [18] Z. Zhai, X. Dai, B. Duo, X. Wang, and X. Yuan, "Energy-efficient UAV-mounted RIS assisted mobile edge computing," *IEEE Wireless Commun. Lett.*, vol. 11, no. 12, pp. 2507–2511, 2022.
- [19] Y. Xu, T. Zhang, Y. Liu, D. Yang, L. Xiao, and M. Tao, "Computation capacity enhancement by joint UAV and RIS design in IoT," *IEEE Internet Things J.*, vol. 9, no. 20, pp. 20 590–20 603, 2022.
- [20] B. Duo, M. He, Q. Wu, and Z. Zhang, "Joint Dual-UAV Trajectory and RIS Design for ARIS-Assisted Aerial Computing in IoT," *IEEE Internet Things J.*, 2023.
- [21] X. Mu, Y. Liu, L. Guo, J. Lin, and R. Schober, "Simultaneously transmitting and reflecting (STAR) RIS aided wireless communications," *IEEE Trans. Wireless Commun.*, vol. 21, no. 5, pp. 3083–3098, 2022.
- [22] M. Ahmed, A. Wahid, S. S. Laique, W. U. Khan, A. Ihsan, F. Xu, S. Chatzinotas, and Z. Han, "A Survey on STAR-RIS: Use Cases, Recent Advances, and Future Research Challenges," *IEEE Internet Things J.*, 2023.
- [23] H. Xiao, X. Hu, P. Mu, W. Wang, T.-X. Zheng, K.-K. Wong, and K. Yang, "Simultaneously Transmitting and Reflecting RIS (STAR-RIS) Assisted Multi-Antenna Covert Communication: Analysis and Optimization," *IEEE Trans. Wireless Commun.*, pp. 1–1, early access, Doi:10.1109/TWC.2023.3 331 706, 2023.
- [24] H. Xiao, X. Hu, A. Li, W. Wang, Z. Su, K.-K. Wong, and K. Yang, "STAR-RIS Enhanced Joint Physical Layer Security and Covert Communications for Multi-antenna mmWave Systems," *arXiv preprint arXiv:2307.08043*, 2023.
- [25] Z. Liu, X. Li, H. Ji, H. Zhang, and V. C. Leung, "Toward STAR-RIS-Empowered Integrated Sensing and Communications: Joint Active and Passive Beamforming Design," *IEEE Trans. Veh. Technol.*, 2023.
- [26] X. Qin, Z. Song, T. Hou, W. Yu, J. Wang, and X. Sun, "Joint Resource Allocation and Configuration Design for STAR-RIS-Enhanced Wireless-Powered MEC," *IEEE Trans. Commun.*, vol. 71, no. 4, pp. 2381–2395, 2023.
- [27] A. Zappone, E. Jorswieck *et al.*, "Energy efficiency in wireless networks via fractional programming theory," *Found. Trends Commun. Inf. Theory*, vol. 11, no. 3–4, pp. 185–396, 2015.
- [28] S. Li, B. Duo, M. Di Renzo, M. Tao, and X. Yuan, "Robust secure UAV communications with the aid of reconfigurable intelligent surfaces," *IEEE Trans. Wireless Commun.*, vol. 20, no. 10, pp. 6402–6417, 2021.
- [29] H. Zhang, N. Shlezinger, F. Guidi, D. Dardari, M. F. Imani, and Y. C. Eldar, "Beam focusing for near-field multiuser MIMO communications," *IEEE Trans. Wireless Commun.*, vol. 21, no. 9, pp. 7476–7490, 2022.
- [30] Y. Zeng, J. Xu, and R. Zhang, "Energy minimization for wireless communication with rotary-wing UAV," *IEEE Trans. Wireless Commun.*, vol. 18, no. 4, pp. 2329–2345, 2019.